Lasers in Medical Science (2019) 34:1421–1431
https://doi.org/10.1007/s10103-019-02742-3

ORIGINAL ARTICLE

Theoretical and experimental modeling of interstitial laser hyperthermia with surface cooling device using Nd^{3+}-doped nanoparticles

D. V. Pominova[1] · I. D. Romanishkin[1] · P. V. Grachev[1] · A. V. Borodkin[1] · A. S. Vanetsev[2] · E. O. Orlovskaya[1] · Yu. V. Orlovskii[1] · I. Sildos[2] · V. B. Loschenov[1] · A. V. Ryabova[1]

Received: 26 December 2017 / Accepted: 30 January 2019 / Published online: 14 February 2019

Abstract

To improve methods of laser hyperthermia for the treatment of bulk malignant neoplasms, an urgent task is the development of techniques and devices that automatically control heating at a given tissue depth and ensure its uniformity. The article proposes the concept of a system for performing hyperthermia with real-time spectroscopic temperature control and surface cooling, which allows to record spectra of diffusely scattered radiation and fluorescent signal from various depths of biological tissues by the means of the variation of the angle and distance between the fiber source of laser radiation and the receiving fiber. Theoretical and experimental modeling of the spatial distribution of diffusely scattered radiation and temperature inside the tissue with a fiber optic device providing surface cooling of the irradiated tissue, and recording spectral information from a given depth in real time, is presented. Simulation of radiation propagation in biological tissues, depending on the distance between the source and the receiver and the angle of their tilt, was carried out using the Monte Carlo method. Modeling of the temperature distribution inside the tissues was carried out by means of a numerical solution of the heat conduction equation. Experimental modeling was carried out on phantoms of biological tissues simulating their scattering properties as well as accumulation of the investigated nanoparticles doped with Nd^{3+} ions. It was shown that inorganic nanoparticles doped with rare-earth Nd^{3+} ions can be used as temperature labels for feedback to the therapeutic laser. According to the results of the theoretical simulation, optimal configurations of the relative arrangement of the fibers were chosen, as well as the optimum surface cooling temperatures for the given power densities. The heating of the phantom of the neoplasm containing the investigated nanoparticles doped with Nd^{3+} ions by laser radiation with an 805-nm wavelength and power density of 1 W/cm^2 up to 42 °C at a depth of 1 cm while maintaining the surface temperature within the limits of the norm was demonstrated.

Keywords Nd^{3+}-doped nanoparticles · Laser interstitial thermal therapy · Near-infrared · Deep biotissue thermal monitoring

Introduction

Interstitional laser-induced hyperthermia based on temperature rise due to the tissue irradiation can be used in order to raise the effectiveness of radio- [1] and chemotherapy [2], as well as the main method of noninvasive tumor therapy [3].

Modern studies of hyperthermia for clinical use focus mainly on optimizing the selectivity, homogeneity, and localization of heating within the tumor, with simultaneous temperature evaluation using non-contact methods, in order to improve the therapeutic effect while minimizing side effects such as overheating of healthy tissues, and to exclude the possibility incomplete destruction of the tumor.

To increase the selectivity of heat delivery to malignant (tumor) sites, special thermal agents are used (also known as heating nanoparticles (HNPs, "nanoheaters")) [4], which can be magnetic and plasmon nanoparticles, nanoparticles doped with rare earth ions, carbon nanotubes or

Electronic supplementary material The online version of this article (https://doi.org/10.1007/s10103-019-02742-3) contains supplementary material, which is available to authorized users.

✉ D. V. Pominova
pominovadv@gmail.com

[1] Prokhorov General Physics Institute of the Russian Academy of Sciences, Vavilov str. 38, Moscow, Russia 119991

[2] Institute of Physics, University of Tartu, W. Ostwaldi st. 1, 50411 Tartu, Estonia

quantum dots [5]. When using nanoheaters, only the temperature of microvolumes surrounding the nanoparticles rises, while the temperature of the entire volume of the irradiated tumor remains the same [6]. Some of the thermal agents not only can be heated by laser radiation, but also have a thermally dependent luminescence, which allows them to be used to locate the tumor and to monitor the local heating temperature throughout the entire hyperthermia procedure [7]. In the recent years, the efforts of researchers are aimed at developing a contactless method for measuring the temperature based on the luminescence rare-earth doped particles (thermoagents) [8]. Carrying out hyperthermia with simultaneous control of the local temperature of nanoparticles makes it possible to select the optimal mode of action in order to ensure the local heating and to avoid overheating the surrounding tissues.

The depth of thermal effect during laser-induced hyperthermia is limited by the depth of light penetration into biological tissues. To achieve maximum depth of the therapeutic effect, laser excitation wavelengths in the NIR range referring to the so-called "biotissue transparency window" are used (first transparency window is 650–950 nm, the second is 1000–1350 nm). In these spectral ranges, the absorption and the scattering of biological tissue components are negligible compared to the visible range, so that light is minimally attenuated on the way to the target. This also reduces the non-selective heating caused by the intrinsic absorption of laser radiation by biological tissues. The maximum depth of laser exposure for human tissues is about a centimeter [9]. The treatment of deeper layers is possible with the use of fiber optic means of delivering laser radiation or with endoscopic methods. A promising direction is also the optical clearing of biological tissues due to a decrease in blood flow by the means of mechanical compression or cooling [10].

The literature suggests there is a great promise in using automated devices that carry out hyperthermia for the treatment of oncological diseases [11]. A number of research groups have demonstrated that magnetic resonance (MR) imaging is effective and accurate for noninvasively assessing temperature changes in tissues associated with absorption of nonionizing radiation [12, 13]. However, technical solutions that allow real-time measurements of temperature fields in the thickness of strongly scattering biological tissues and regulate the degree of heating of different zones are lacking [14]. For contactless temperature evaluation, by far, the most frequently used devices are thermal cameras, which, hovewer, measure only the surface temperature. The methods of spectroscopic temperature estimation described in the literature also use spectra obtained from the surface area of irradiation, so the temperature at depth remains unknown [15].

The article describes the concept of a system for conducting hyperthermia with real-time temperature control, which allows to record spectra of diffusely scattered radiation from various depths of biological tissues by the means of variation of the angle and distance between the fiber source of laser radiation and the receiving fiber.

For contactless temperature monitoring, the composite NPs doped with Nd^{3+} ions with absorption and luminescence bands in the NIR range providing the maximum depth of sounding of biological tissues were used as thermal agents.

The system for conducting hyperthermia consists of a laser source of the near-infrared spectral range and a fiber optic device for contact irradiation, combined with a spectro-analyzer, which makes it possible to detect diffusely scattered radiation and luminescence. The device is a special holder for the optical fiber, through which the exciting laser radiation is provided, equipped with a sapphire window with a thermal sensor and a cooling system [16].

The construction of a fiber optic device for contact illumination makes it possible to vary the angle of inclination of the receiving fiber relative to the normal to the surface of the irradiated region and the distance between the source and the receiving fiber in order to regulate the depth of sounding [17]. To optimize the design of the device, the photon-tissue interaction had to be evaluated. To do this, we simulated the dependence of the depth of sounding on the distance between the fibers and the angle of inclination of the receiving fiber relative to the normal to the irradiated surface using the Monte Carlo method. In order to create a model based on the results of the simulation, the characteristic slope angles of the fibers relative to the normal to the biotissue (0°, 30°, 45°) and the distances from the center of irradiation (1.5–2.5 cm) were chosen. For the established optimal configurations, further experimental studies of the intensity of laser radiation diffuse scattering and luminescent signal on phantoms of biological tissues were carried out. The use of the cooling system allows increasing the depth of thermal effect on biological tissues and avoiding overheating the surface, where the power density of laser radiation is maximal. To simulate the spatial distribution of temperature in biological tissues, the numerical solution of heat equation (finite difference method, PDE ToolBox, Matlab) was used. Simulation allowed determining the characteristics of the exciting radiation at which the power density in the depth of the tissue is sufficient to heat the composite NP accumulated in the neoplasm but not to damage the surrounding tissues. It was also demonstrated that, without the use of a cooling device, surface superheating occurs. Optimal cooling temperatures of the sapphire window that allow increasing the depth of thermal effect and providing even heating of the illuminated area for various excitation light power densities have been established.

Materials and methods

Theoretical modeling

Monte Carlo method for modeling the dependence of the sounding depth of biological tissues on the configuration of fibers

The aim of the simulation was to establish the dependence of the laser sounding depth of biological tissues on the distance and angle between optical fibers, one of which is a source of photons, and the other a receiver. The use of such a geometry allows varying the depth of sounding z by changing the distance and angle between the fibers. In accordance with the diffusion theory, the region of the most probable passage of photons from the detector to the receiver in a semi-infinite medium has the form of a "banana" [18]. We assume the depth of sounding to be the distance from the surface of the irradiated object to the maximum intensity in the region of the most probable passage of photons between the fibers [19–21]. The intensity distribution maximum in the medium in y-z cross section at $y = 0$ (based on symmetry) can be found using formula [17, 22]:

$$z(r) = \sqrt{\frac{1}{8}\left[\sqrt{\left(x^2 + (r-x)^2\right)^2 + 32x^2(r-x)^2} - x^2 - (r-x)^2\right]}. \quad (1)$$

However, the diffusion theory is applicable only for the case of isotropically scattering media with negligible absorption. And, therefore, for biological systems, it is necessary to use numerical methods or Monte Carlo simulations, which, although not allowing us to obtain a solution in a compact analytical form, give the required results.

In order to describe media characterized by a large scattering anisotropy, the transfer theory is used. The transfer equation describes the change of beam intensity as the result of absorption and scattering in the medium. Beam intensity in a point is described as a sum of two components. The first, collimated, describes the light that has not been absorbed or scattered once. The second, diffuse, describes the light that was involved in the scattering process. The main difficulty consists in determining the diffused component because photon scattering is of random nature. In order to determine the diffused component and to model the transfer of light between two fibers in a two-dimensional medium, the Monte Carlo method was used. It is based on numerical modeling of photon transfer in scattering medium. The absorption and scattering are taken into account throughout the path of photons from the point of entry into the sample and until their absorption or exit from the sample.

In this work, the propagation of laser radiation with a wavelength of 805 nm from two optical fibers in an array of phantoms with a concentrations of fat emulsion (Lipofundin®) corresponding to the scattering properties of brain tissue (0.4%), muscle tissue (1%), and skin (1.6%) was simulated using the Monte Carlo method. A series of simulations were performed in which the distance between the fibers varied from 0.5 to 75 mm, and the angle of inclination of the fibers varied from 0 to 75°. For the simulation, MClight software described in [17] was refined to allow changing the angle of fibers inclination. The simulation was performed for the case of fibers with an aperture of 0.22 and optical fiber thickness of 250 μm. Optical parameters of the model medium are presented in Table 1. For the case of phantom models containing the studied nanoparticles, the effective scattering and absorption parameters were calculated (see Supporting info). Since the maximum allowable concentration of injected nanoparticles is 5 mg/kg, they practically do not affect the optical properties of the studied phantoms (a fraction of a percent difference).

The calculations results are presented in the form of an image of the light field formed by the propagation of photons in a given medium. The image has 16-bit dynamic range of color, which allows catching small changes in brightness of the light field. The search for a region of space between fibers in which photons pass with highest probability is as follows. Regions which photons most often pass through are brighter. Therefore, if we look for points on the image that are brightest, we can obtain information about where the photon flux density is highest. Thus, in the region where the "banana" is supposed to be located, the brightness maximum is searched for in each vertical section between the fibers. The result is the central line of the "banana" shape. In order to find the thickness of the "banana" in each vertical section, the range of intensity values from the brightness maximum to half the maximum brightness upwards and downwards is sought. The located area is colored, and the obtained results can be saved in a graphical file.

Theoretical modeling of the exciting radiation parameters for effective hyperthermia in the depth of biological tissue using the cooling device

Simulation for the selection of optimal parameters of the exciting radiation and the temperature of the cooling device was carried out for the case of real biological tissues based on the skin. Simulation of heating under the effect of laser radiation was carried out for the case of irradiation with a laser with a wavelength of 805 nm, focused in a spot of 1 cm^2.

The choice of parameters for modeling the interaction of laser radiation with biological objects was carried out on the basis of information on the skin physiology [23, 24]. The skin consists of three main layers: the epidermis, which includes the stratum corneum and the living epidermis, dermis, and

Table 1 Modeling coefficients

Intralipid concentration, %	0.4	1.0	1.6
Scattering coefficient at 805-nm wavelength m_s [cm^{-1}]	5.3	13.3	21.3
reduced scattering coefficient at 805-nm wavelength m_s [cm^{-1}]	2.50	6.25	10.00
Anisotropy factor g		0.53	
Absorption coefficient at 805-nm wavelength m_a [cm^{-1}]	0.012	0.031	0.050

hypodermis. Approximately 5–7% of the incident light is reflected by the stratum corneum. The main scatterers in the biotissue are collagen and elastin fibers in the dermis, as well as keratin and melanin in the epidermis. The main absorbers of radiation are melanin in the epidermis, and water and hemoglobin in the dermis. By using a wavelength of 805 nm, absorption and heating will occur mainly in the dermis region, since it contains the maximum number of water molecules that are the main absorbers at this wavelength. The removal of heat from the site of irradiation and natural cooling occurs due to thermal conductivity, convective heat transfer or thermal radiation, and also due to blood flow. When simulating the cooling of the irradiated tissue surface with the help of the developed device, heat transfer between the biotissues and the sapphire window was also taken into account at various cooling temperatures of the window.

The dependence of the temperature spatial distribution in biological tissues from time is described by the differential heat equation:

$$\rho \cdot c \cdot \frac{\partial T(\vec{r},t)}{\partial t} = \mathrm{div}\left(k \cdot \mathrm{grad}\, T(\vec{r},t)\right) + Q(\vec{r}) + S(\vec{r}), \quad (2)$$

where ρ–density, c–specific heat of medium, t–time, k–thermal conductivity, $Q(r)$ –volumetric density of heat sources in the medium, and $S(r)$–heat transfer due to blood flow. Blood can absorb or release heat depending on how its temperature correlates with the temperature of the surrounding tissue. The term $S(r)$ can be written as:

$$S\left(\vec{r}\right) = \rho \cdot c \cdot p_b \cdot v_b (T_b - T), \quad (3)$$

where ρ_b–blood density, v_b–blood flow density in tissues, and T_b–blood temperature.

The generation of heat inside the tissue when irradiated with a laser beam can be calculated as:

$$Q(r,z) = m_a \cdot (1-R) \cdot I_o \cdot e^{\left(-r^2/2\sigma(z)\right)} \cdot e^{\left(-\left(m_a + m_s'\right)z\right)}, \quad (4)$$

$$r = \sqrt{x^2 + y^2}, \quad (5)$$

$$R = \left(\frac{n-1}{n+1}\right)^2, \quad (6)$$

where I_o–intensity of the incident laser radiation, σ–Gaussian distribution, m_a and m_s–absorption and scattering coefficients with anisotropy, respectively, R–reflection coefficient taking into account the reflection of the incident radiation from the skin surface, n–refractive index, and x, y–coordinates. To take into account the effect of the introduction of the studied nanoparticles on the heating of biological tissues under the laser irradiation, effective thermo-physical parameters were calculated (see Supporting info).

For simulation, the numerical solution of heat equation (finite difference method, PDE ToolBox, Matlab) was used.

Experimental section

Synthesis of composite LaF_3 nanoparticles doped with Nd^{3+} ions

In this work, the composite core-shell LaF_3@$DyPO_4$ nanoparticles doped with Nd^{3+} ions synthesized by the co-precipitation method in aqueous solutions with subsequent hydrothermal-microwave treatment were used as thermal agents [25]. The concentration of Nd^{3+} ions was 1%.

Optical phantoms of biological tissues imitating their scattering and luminescent properties

The solutions of fatty emulsions were used for modeling of the biological tissues scattering properties [26]. The optical properties of fat emulsions are described in detail in the literature [27, 28]. In this work, a fat emulsion for parenteral nutrition on a water basis Lipofundin® MST/LST 20% (B.Braun Melsungen, Germany) was used. To create solid phantoms, Lipofundin® aqueous solution was added to a previously boiled 1% agarose solution, poured into a mold, and cooled until solidified. The size of the investigated cylindrical scattering phantoms was 10 cm in diameter, and the height was varied from 4 to 8 cm. To study backward diffuse scattering, an array of phantoms with a concentrations range of fat emulsions from 0.2 to 3% was prepared corresponding to the scattering properties of brain tissue (0.4%), skin (1.6%), and muscle tissue (1%). The studied composite NPs (at a concentration of 5 mg/l) were used as the luminophore. The phantom simulating the neoplasm was a cylinder 0.5 cm in height and 1 cm in diameter and contained LaF_3:Nd^{3+} nanoparticles. It was

placed inside a scattering phantom that simulates healthy tissues, and its depth from the surface was controlled in the range from 5 to 10 mm.

Registration of backward diffuse scattering and luminescence spectra with a surface cooling device for contact irradiation

The surface cooling device for contact irradiation (Fig. 1) consists of a laser source connected by an optical fiber (1) to a cooling unit (2), using an SMA fiber attachment, a sapphire window, and an electronic Peltier element. A sapphire window equipped with a thermal sensor is connected to the cooled side of the Peltier element, and the hot side of the Peltier element is equipped with a radiator with a large surface and a hole for the laser irradiation. The cooling is controlled by electrical unit [16]. The device is equipped with a nozzle (3) with ports in which the receiving fiber (4) is fixed. The nozzle allows the receiving fiber to be positioned at different angles and at different distances from the center of irradiation using different port groups.

The backward diffuse scattered and the luminescent signals were investigated when excited by an 805-nm wavelength laser LFT-805-01-BIOSPEC (Biospec, Russia). The working plane was illuminated using an optical fiber fixed in the SMA connector of the surface cooling device for contact irradiation at a distance of 2 cm from the surface. The irradiated area was 1 cm^2. The laser power at the exit from the sapphire window of the cooling device was varied from 0.3 to 2 W. To obtain the backward diffuse scattering of the laser and the luminescence spectra, Raman-HR-TEC spectrometer was used (StellarNet, USA). The receiving fiber was positioned at a distance of 1.5–2.5 cm from the center of the sapphire window at angles 0°, 30°, and 45° from the surface normal.

The evaluation of the temperature using ratiometric spectroscopic method by the change in the Nd^{3+} luminescence spectrum

The ratio of the luminescence intensities from the Nd^{3+} ion $^4F_{3/2}$ excited state Stark sublevels, used as the temperature-dependent parameter Δ, can be calculated in accordance with the Boltzmann distribution [29]:

$$\Delta = \frac{I_2}{I_1} = B \cdot \exp\left(\frac{-\Delta E}{k_B T}\right) \quad (7)$$

where I_2 and I_1–intensities of transitions from the Nd^{3+} ion $^4F_{3/2}$ excited state Stark sublevels, k_B–Boltzmann constant, ΔE–the energy gap between the first and the second Stark sublevels of $^4F_{3/2}$ state, T–temperature, and B–constant determined by the degeneracy of the state and the probability of spontaneous relaxation.

Thus, for a known energy gap between the Stark sublevels, which is 42 cm^{-1} for the LaF_3 matrix [30], a calibration curve can be constructed that makes it possible to calculate the change in the intensities ratio to the real temperature value. The procedure is described in detail in [31]. In addition, an independent monitoring of the tissues phantoms heating temperature using an infrared thermal camera JADE MWIR SC7300M (CEDIP, France) was carried out.

Results and discussion

Using the Monte Carlo method, the propagation of an 805-nm laser radiation in biological tissues was simulated for two optical fibers located at various distances from one another and inclined at various angles relative to the normal of the surface. The results of the calculations are presented as an image on which the light field formed during the passage of photons through a given medium is displayed (Fig. 2a, c). A series of calculations was performed for a set of fiber configurations, which made it possible to establish the dependence of the biotissue optical probing depth on the distance between the fibers (Fig. 2b), and their direction angle relative to the normal of the surface (Fig. 2d).

It was estimated that the optical probing depth has a power-law dependence on the distance between the fibers (Fig. 3b) for all fat emulsion concentrations. At the same time, the depth of sensing increases with decreasing concentration of the fat emulsion due to reduced scattering. However, it should be

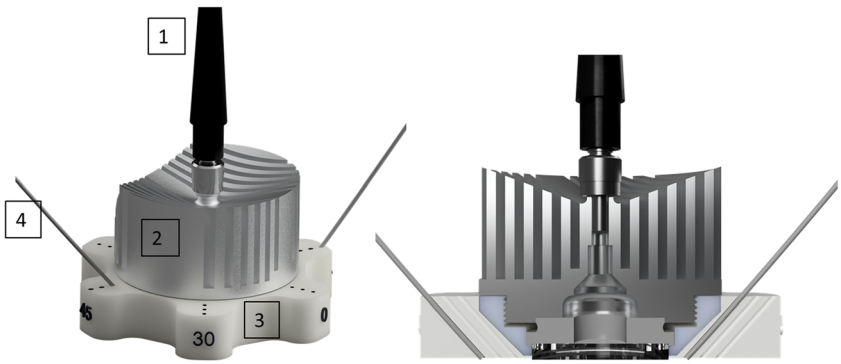

Fig. 1 Fiber optic device for controlled local laser hyperthermia: (1) optical fiber supplying therapeutic laser radiation through the device for forced cooling of the surface (cooler, 2) (3) nozzle on the cooler for positioning of receiving scattered laser radiation and luminescence fibers (4) at various angles and distances from the center of irradiation

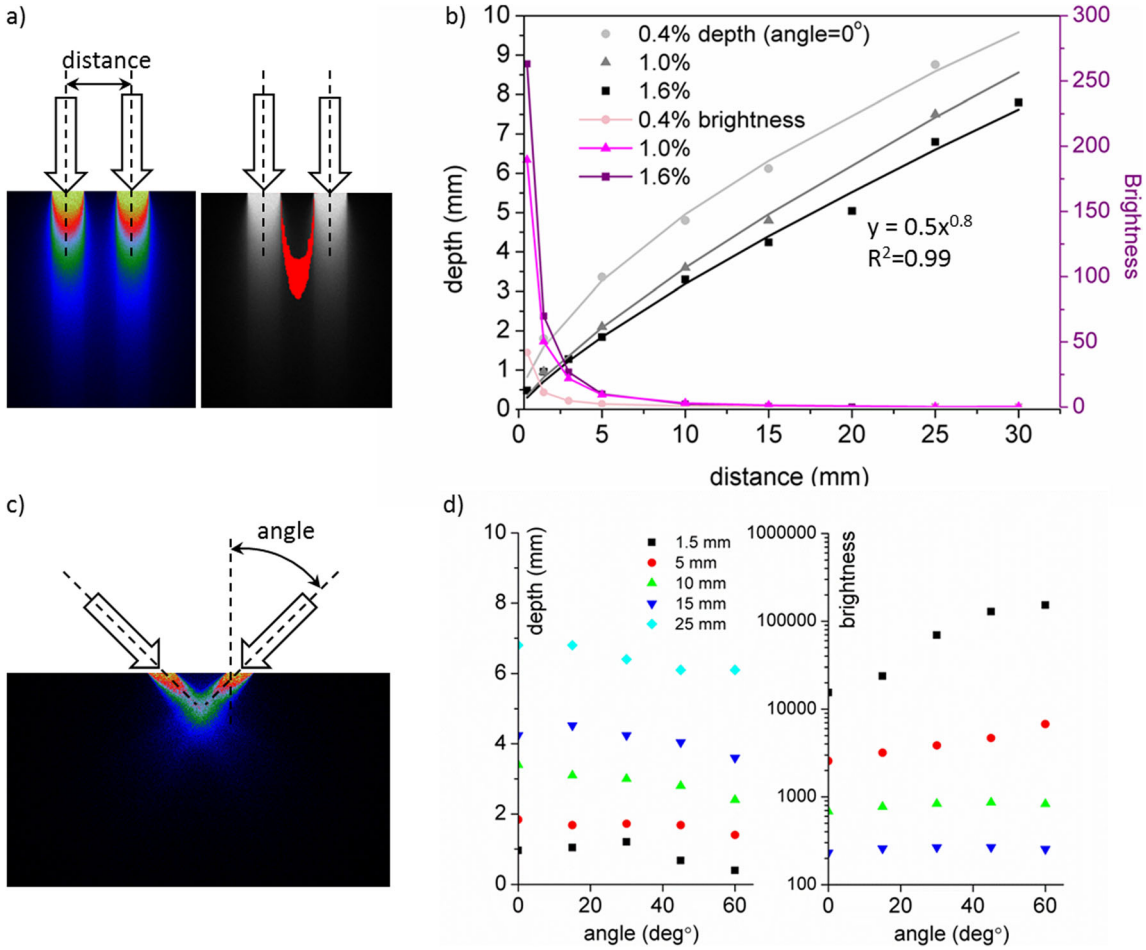

Fig. 2 **a** The light field produced when photons pass through the 1.6% fat emulsion solution for distance between fibers 0.5 mm and the slope angle 0° in the pseudocolor and the calculated area of the most probable photon migration path (shown in red). **b** The dependence of optical probing depth and brightness of the detected signal on the distance between the fibers and fat emulsion concentration. **c** The light field produced during the passage of photons in biotissue for distance between the fibers 5 mm and slope angle of 45°. **d** The dependence of optical probing depth and the brightness of the detected signal on the angle of inclination of the fibers relative to the normal of the surface at a fixed distance

noted that along with an increase in the probing depth, the brightness of the detected signal decreases with the decrease of the fat emulsion concentration. The nature of the brightness dependence on the distance between the fibers does not change with a change in the fat emulsion concentration. With an increase in the distance from 1 to 10 mm, a sharp increase in the depth of sounding is observed, at distances greater than 10 mm, the depth increase is slower. Since it is necessary not only to probe the biological tissues with laser radiation, but also to excite fluorescence in the depth of the tissues, it is also important to estimate the power density as a function of depth. Based on the experimental data, the power density of 0.5 W/cm^2 is sufficient to excite the Nd^{3+} luminescence. Based on the pumping power requirements, the optimal distance between the fibers is 15 mm. With such a configuration, the provided fluorescence radiation optical probing depth is about 4 mm. In order to further increase the probing depth, it is necessary to increase the distance between the fibers. However, it should be noted that, in this case, the brightness of the detected signal will be significantly reduced and a longer accumulation time may be required. In the case where the scattering is lower, the fibers should be located closer to each other in order to obtain sufficient brightness.

Figure 3d shows the characteristic dependences of the biotissue optical probing depth and the brightness of the detected signal on the fibers slope angle relative to the normal of the irradiated surface, with a fixed distance between the fibers. It can be seen that the dependence of the probing depth on the slope angle is less strong than the dependence on the distance. An addition, the probing depth decreases with the angle increase. On the other hand, as the angle is increased, the intensity of the detected signal also increases. The strongest dependence of brightness on the slope angle is observed for small distances between fibers. Since, as was shown above, the concentration of the fat emulsion affects only the absolute values of depth and brightness and does not affect the dependence, the simulation was performed for 1.0% of the fat emulsion that is closest to real conditions (skin scattering).

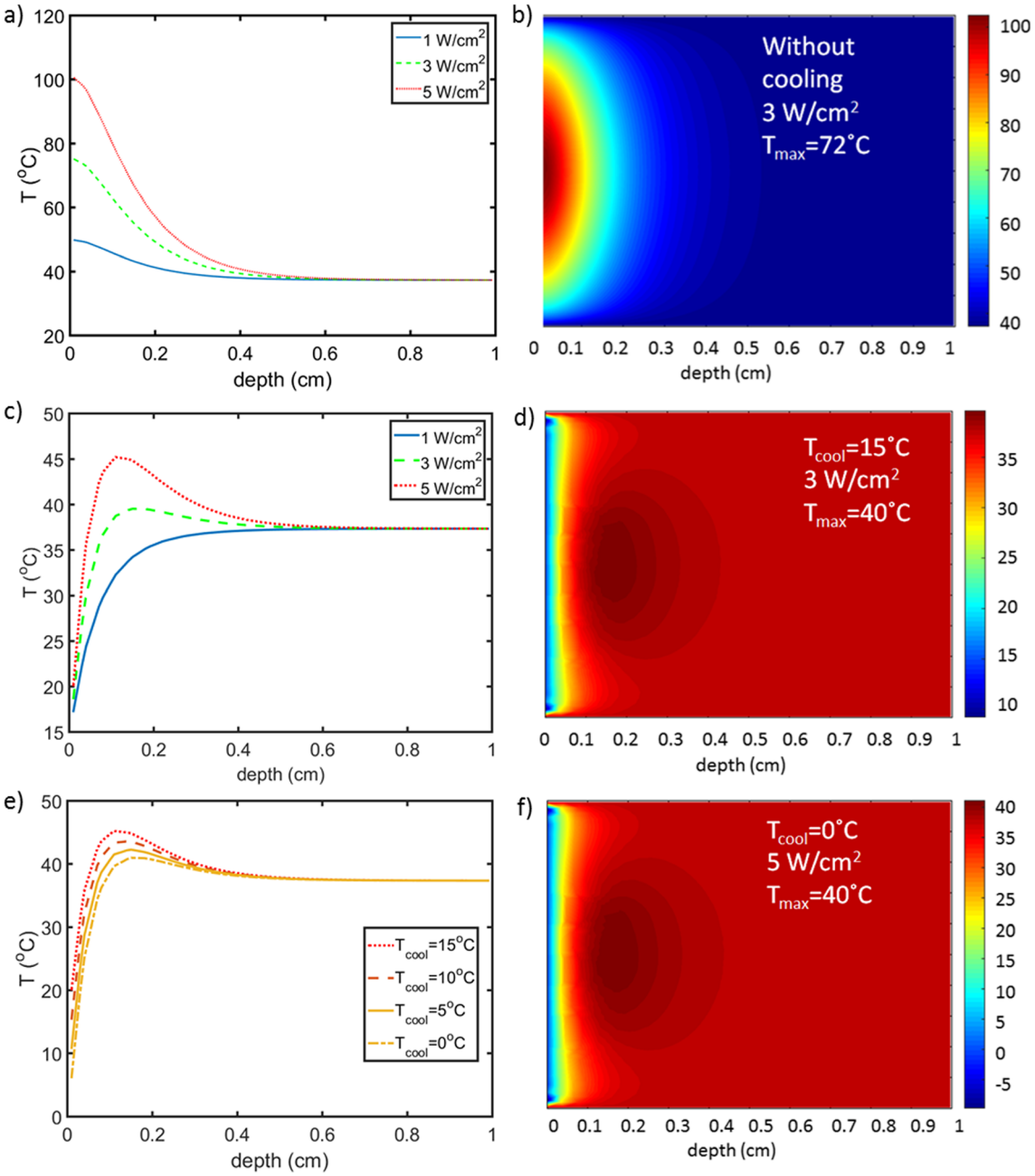

Fig. 3 **a** The dependence of temperature on the depth of biological tissue at various pumping power densities without use of surface cooling. **b** The temperature distribution profile in the depth of biological tissues at 3 W/cm^2 power density without use of cooling. **c** The dependence of temperature on the depth of biological tissue at different power densities of the exciting radiation with use of cooling (T_{cool} = 15 °C). **d** The temperature distribution profile in the depth of biological tissues at 3 W/cm^2 power density with the use of cooling (T_{cool} = 15 °C). **e** Dependence of temperature on the depth of biological tissue at 5 W/cm^2 power density using surface cooling with different the cooler temperature. **f** The temperature distribution profile in the depth of biological tissues at 5 W/cm^2 power density with the use of cooling (T_{cool} = 0 °C)

Thus, in order to obtain a signal of sufficient intensity from the maximum depth in the biological tissue, it is most sensible to use optical fibers located at a long distance from each other (1.5–2 cm) but at a small angle to the surface (15°–45°). Based on the simulation results, the characteristic fiber slope angles relative to the normal of the biotissue were chosen to create a model of the fiber optic device for hyperthermia: 0°, 30°, 45° angles and distance 1.5–2.5 cm from the center of irradiation. These values are optimal for the probing depth of up to 1 cm in the tissues of the meninges, subcutaneous fat, and mammary gland tissue.

Theoretical modeling of the laser excitation parameters for effective hyperthermia in the thickness of biological tissue has shown that, without cooling, even at 1 W/cm^2 power density, a

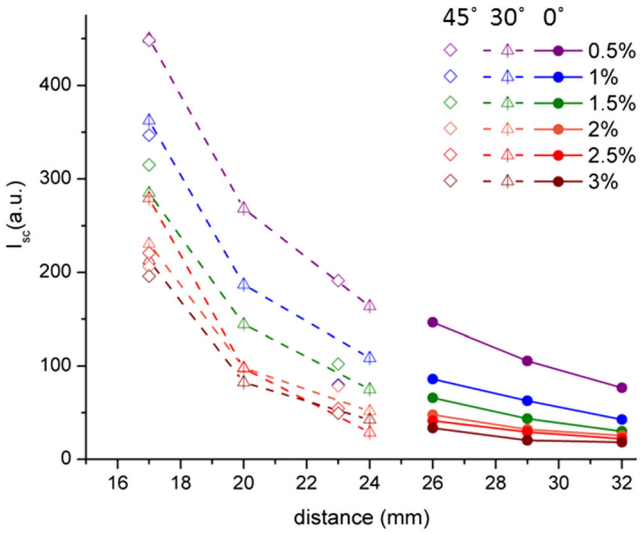

Fig. 4 The dependence of the scattered laser radiation intensity for a number of concentrations of Lipofundin® on the distance between the receiving and irradiating fibers for different slope angles of the receiving optical fiber to the normal of the surface under investigation: 0° (circle, solid line), 30° (hollow triangle, dashed line), and 45° (diamond)

sufficiently strong superheat of the surface was observed, and the surface temperature reached 50 °C (Fig. 4a). As the power density increases, the heating becomes more critical, at 3 W/cm^2 the surface temperature reaches 72 °C, while the temperature in the depth of tissues remains unchanged. The dependence of temperature on depth and the temperature distribution profile in biological tissues for 3 W/cm^2 power density of without cooling are shown in Figs. 3a, b, respectively.

At the next stage, the heating was modeled depending on the laser excitation power density at a fixed cooler temperature of 15 °C (Fig. 3c). From the obtained temperature dependences on the depth, it can be seen that at a power density less than 5 W/cm^2, the surface does not overheat, and the maximum of heating is at a depth of 0.1 cm. The corresponding temperature distribution profile in the depth of biological tissues is given in Fig. 4d. However, for higher power densities, the overheating is still observed. Due to this, we simulated the heating of biological tissues for a fixed excitation power density 5 W/cm^2 and various cooling temperatures (Fig. 3e).

From the data obtained, it follows that using 5 W/cm^2 power density requires very low cooling temperatures ($T_{cool} = 0$ °C) in order to obtain a temperature distribution in the thickness of the tissues similar to that obtained at 3 W/cm^2 and the window cooling at 15 °C. In this case, the surface temperature will be very low, which can also lead to side effects. The contour plot of the temperature distribution profile in the depth of biological tissues at 5 W/cm^2 pumping power density and cooler temperature of 0 °C is given in Fig. 3f). From the contour plots, it can be seen that, in addition to the minimization of overheating, the use of surface cooling also allows shifting the area of thermal influence deeper into the tissue.

When using averaged parameters for the tissue containing the NP, the heating temperature remains almost unchanged and is 50 °C for the surface at 1 W/cm^2. However, if the simulation is carried out for LaF_3:Nd@$DyPO_4$, using the thermal parameters for LaF_3, which is the core of all NPs and the average absorption value for Nd and Dy (3.6), calculated by taking into account the fraction of Dy ions in the shell, the material will be heated to 57 °C under 1 W/cm^2 excitation. Thus, we can assume that local heating regions arise around the NPs, which is indirectly confirmed by the results of our experimental studies, as well as by literature [32].

Experimental modeling of local laser hyperthermia with the use of surface cooling device for contact irradiation and composite LaF_3:Nd^{3+} nanoparticles was carried out on biological tissue phantoms simulating their scattering properties, as well as the accumulation of the investigated luminophore. For the selected configurations of optical fibers positions, further experimental studies of the dependences of the intensity of laser radiation diffuse scattering and the luminescence signal on the fiber slope angle (0°, 30°, and 45°) from the surface normal, on the distance between the source and the receiving fiber, and also on the simulated biotissues scattering characteristics were carried out.

The backward diffuse scattering is an important characteristic of biotissues that allows evaluating the tissue integrity. The change in backward diffuse scattering upon heating may indicate coagulation or carbonization. To perform hyperthermia in vivo, positions of the receiving fiber should be selected in a way that provides the maximum intensity of the laser radiation backscattered diffuse signal, and, consequently, a higher sensitivity to the change in the properties of irradiated tissues.

As a result of experimental investigations, the dependence of the intensity of scattered laser radiation on the distance between the irradiating and receiving optical fibers for different slope angels and concentrations of Lipofundin® was obtained (Fig.4).

As can be seen from the obtained dependences, the closer the receiving fiber is to the irradiated region, the more intense is the detected signal. At the same time, the slope of the fiber has practically not affected the intensity of the laser backward diffuse scattering. These results are in good agreement with the Monte Carlo simulation. By increasing the percentage of Lipofundin® in phantom, the probability of scattering increases and, consequently, the mean free path of photons decreases. In this regard, a decrease in the detected signal intensity is observed as the concentration of Lipofundin® increases.

For a phantom, which simulated the nanoparticles accumulation in the neoplasm, the dependences of the luminescence intensity of the investigated composite nanoparticles on their occurrence depth in the biotissue were obtained. For experimental study, a neoplasm phantom was placed inside a scattering phantom that simulates healthy tissue, and its depth

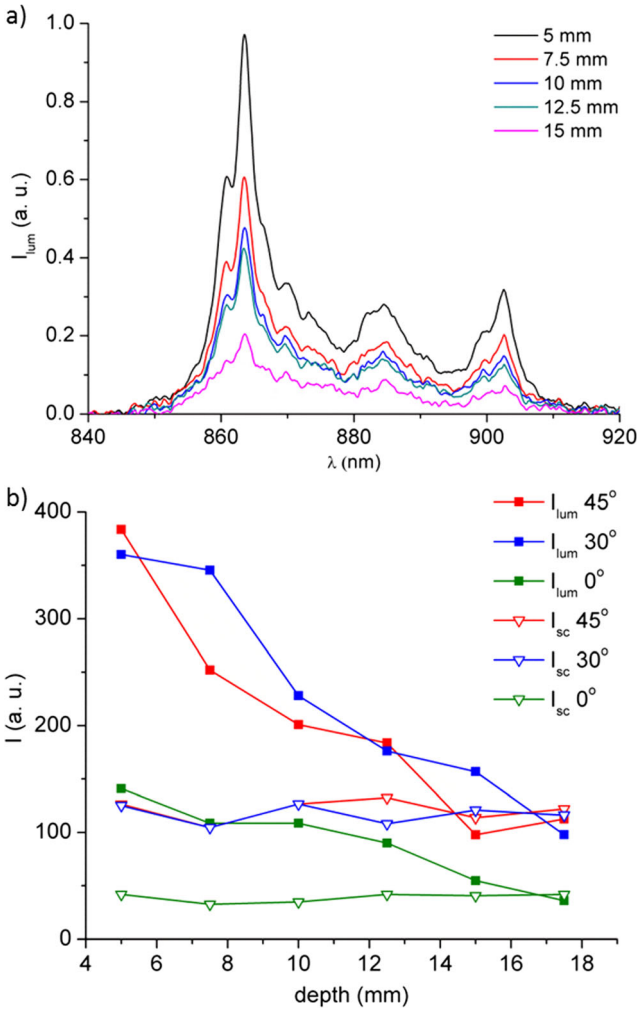

Fig. 5 **a** The change of the luminescence spectrum with increasing occurrence depth of the optical phantom simulating the neoplasm containing $LaF_3:Nd^{3+}$. **b** The dependence of the luminescence intensity (markers with filling) and scattered laser radiation (hollow markers) on the occurrence depth of the phantom that simulates the neoplasm, for different slope angle between the receiving optical fiber and the normal to the surface under investigation: 0° (green lines), 30° (blue lines), and 45° (red lines)

from the surface was controlled in the range from 5 to 10 mm. The distance between the fibers 24 mm was used to record the luminescence spectra and the slope angle of the receiving fiber was varied in the 0–45° range. An example of the luminescence spectrum change with the increase of the occurrence depth of the phantom with the investigated composite nanoparticles is shown in Fig. 5a. The obtained dependences of the luminescence intensity on the occurrence depth for each slope angle of the receiving optical fiber are shown in Fig. 5b.

It can be seen that the intensity of the luminescent signal decreases with increasing occurrence depth of the neoplasm phantom, but remains sufficient for detection up to a depth about 1 cm. The intensity of the signal is higher for the case of using inclined fibers, which also agrees with the results of the simulation. The measured luminescence intensity is sufficient for detecting the accumulation of nanoparticles in the neoplasm, while all the lines necessary for thermometry are visible in the luminescence spectrum. The intensity of backward diffuse scattering with an increase in the depth of occurrence changes much more weakly than the intensity of the detected luminescent signal, and can be used to monitor the state of soft tissues during hyperthermia, even with a large occurrence depth of the neoplasm.

The temperature distribution measurements during the hyperthermia of neoplasm phantoms lying inside a scattering media at different depths from the surface were carried out on solid phantoms prepared according to the procedure described in the "Materials and methods" section. Based on the modeling results and experiments to obtain the maximum signal intensity, the slope angle to normal of the receiving fiber 30° and the distance 24 mm from the center of the sapphire window of the cooling device were used.

The dependence of the heating temperature on the excitation power for the neoplasm phantom, lying at a depth of 5 mm, 7 mm, and 10 mm from the surface, was investigated. The evaluation of the heating temperature was carried out by the spectroscopic ratiometric method described in the "Materials and methods" section. In addition, the phantom was cut along the central axis and the phantom heating temperature was independently estimated using the infrared thermal camera. Room temperature of 23 °C, measured using a thermal camera, was selected as a starting point for all studied samples. Between the measurements, the samples were cooled until they reached room temperature.

The values of the neoplasm phantom heating temperature obtained by the infrared thermal camera are given in the Table 2. According to the results obtained using the thermal camera, the maximum heating temperature of the neoplasm phantom containing the investigated nanoparticles located at a depth of 1 cm from the surface was 27 °C under 1.7 W/cm^2 laser power density. The heating of phantoms that did not contain the investigated nanoparticles was negligible. The use of a surface cooling system can significantly reduce the heating of tissues at high power densities. For example, when 1.7 W/cm^2 power density is used, the heating temperature of neoplasm reaches 26–27 °C.

The results of temperature estimation by spectroscopic method using $LaF_3:Nd^{3+}$ luminescence are also presented in the Table 2. The maximum temperature calculated spectroscopically for neoplasm phantom irradiated by an 805-nm continuous wave laser with 1 W/cm^2 power density was 56 °C for a depth of 5 mm and 54 °C for a depth of 10 mm.

Weak heating of deep-lying neoplasms is associated with a strong decrease of excitation power density in the depth due to scattering. By comparing the results obtained with a thermal camera and a spectroscopic technique, it can be seen that the temperature values obtained with a thermal camera are significantly underestimated. This is associated with the cooling of

Table 2 Dependence of the heating temperature of neoplasm phantom lying at different depths from the surface on the excitation power density

T, °C (spectral method)				
Depth, mm	$P = 0.5$ W/cm^2	$P = 0.7$ W/cm^2	$P = 1$ W/cm^2	$P = 1.7$ W/cm^2
5	43	46	48	56
7	35	40	46	55
10	25	33	42	54
T, °C (thermal camera)				
Depth, mm	$P = 0.3$ W/cm^2	$P = 1$ W/cm^2	$P = 1.7$ W/cm^2 with cooling	$P = 1.7$ W/cm^2
10	24	26	26	27
10, control without NPs	23	25	24	24

the phantom surface due to convection and evaporation of water from phantom, as well as with the nanoparticle heating localization. The spectroscopic technique makes it possible to estimate the direct heating temperature of the particles themselves and their nearest microenvironment and to measure the temperature deep in biological tissue.

Conclusions

Experimental studies carried out using a system for hyperthermia with real-time temperature control and cooling of the irradiated surface have shown great promise of the developed concept. Using the optimal configurations of the optical fibers location (angle and distance), determined by the results of theoretical and experimental modeling, it was possible to reliably detect backward diffuse scattering and a luminescent signal from the depth of about 1 cm. In this case, all the Nd^{3+} ions spectral lines necessary for thermometry were observed in the luminescence spectrum in real time.

A comparison of the results of temperature ratiometric determination from the spectra with measurements carried out using a thermal camera has shown that the ratiometric method allows estimating the direct heating temperature of the particles themselves and their nearest microenvironment deep in biological tissue, in contrast with thermal camera measurements, which give information only about the surface temperature.

The use of cooling device helps avoiding overheating the surface, even at sufficiently high excitation power densities (up to 3 W/cm^2), and also shift the area of therapeutic influence deeper into the biotissue. With the help of a system for hyperthermia with real-time temperature control and cooling of the irradiated surface, the heating temperature of the neoplasm phantom containing the investigated LaF_3:Nd^{3+} nanoparticles reached 42 °C at a depth of 1 cm under a 805 nm laser irradiation with 1 W/cm^2 power density, while maintaining the surface temperature within normal limits.

Funding This researched received financial support from the Russian Science Foundation (project N 17-72-20186).

Compliance with ethical standards

Conflict of interest The authors declare that they have no conflict of interest.

Ethical approval The experiments presented in the manuscript do not contain studies with human participants or live animals performed by any of the authors. The studies were performed on biological tissue phantoms.

Informed consent It does not apply, since the study was developed on biological tissue phantoms.

Publisher's note Springer Nature remains neutral with regard to jurisdictional claims in published maps and institutional affiliations.

References

1. Van der Zee J, Gonzalez DG, van Rhoon GC et al (2010) Comparison of radiotherapy alone with radiotherapy plus hyperthermia in locally advanced pelvic tumours: a prospective, randomised, multicenter trial. Lancet. https://doi.org/10.1016/S0140-6736(00)02059-6
2. Marangon I, Silva AAK, Guilbert T, Kolosnjaj-Tabi J, Marchiol C, Natkhunarajah S, Chamming's F, Ménard-Moyon C, Bianco A, Gennisson JL, Renault G, Gazeau F (2017) Tumor stiffening, a key determinant of tumor progression, is reversed by nanomaterial-induced photothermal therapy. Theranostics. https://doi.org/10.7150/thno.17574
3. (2013) Hyperthermia: using heat to treat cancer. National Comprehensive Cancer Network. www.nccn.com/component/content/article/60-treatment/932-hyperthermia-treatment.html Accessed June 17 2013
4. Leitgeb N et al (2016) Exposure of non-target tissues in medical diathermy. Bioelectromagnetics 31:12–19
5. Kaur P, Aliru ML, Chadha AS, Asea A, Krishnan S (2016) Hyperthermia using nanoparticles – promises and pitfalls. Int J Hyperth. https://doi.org/10.3109/02656736.2015.1120889
6. Kang P, Chen Z, Nielsen SO, Hoyt K, D'Arcy S, Gassensmith JJ, Qin Z (2017) Molecular hyperthermia: spatiotemporal protein unfolding and inactivation by nanosecond Plasmonic heating. Small. https://doi.org/10.1002/smll.201700841
7. Carrasco E et al (2015) Intratumoral thermal reading during photothermal therapy by multifunctional fluorescent nanoparticles. Adv Funct Mater 25(4):615
8. Rocha U, Hu J, Rodríguez EM, Vanetsev AS, Rähn M, Sammelselg V, Orlovskii YV, Solé JG, Jaque D, Ortgies DH (2016) Subtissue imaging and thermal monitoring of gold nanorods through joined

encapsulation with Nd-doped infrared-emitting nanoparticles. Small. https://doi.org/10.1002/smll.201600866
9. Helmchen F, Denk W (2005) Deep tissue two-photon microscopy. Nat Methods 2:932–940
10. Bashkatov AN, Tuchin VV, Genina EA, Sinichkin YP, Yanina IY (2010) Optical clearing of tissues: benefits for biology, medical diagnostics, and phototherapy. In Tuchin VV (ed.) Handbook of Optical Biomedical Diagnostics, Second Edition, Volume 2: Methods. SPIE Press Bellingham, Washington USA
11. Issels R, Kampmann E, Kanaar R, Lindner LH (2016) Hallmarks of hyperthermia in driving the future of clinical hyperthermia as targeted therapy: translation into clinical application. Int J Hyperth. https://doi.org/10.3109/02656736.2015.1119317
12. Davis RM, Viglianti BL, Yarmolenko P, Park JY, Stauffer P, Needham D, Dewhirst MW (2013) A method to convert MRI images of temperature change into images of absolute temperature in solid tumors. Int J Hyperth 29(6):569–581. https://doi.org/10.3109/02656736.2013.790091
13. Wyatt C, Soher B, Maccarini P, Charles HC, Stauffer P, MacFall J (2009) Hyperthermia MRI temperature measurement: evaluation of measurement stabilization strategies for extremity and breast tumors. Int J Hyperth 25(6):422–433. https://doi.org/10.1080/02656730903133762
14. Saccomandi P, Schena E, Silvestri S (2013) Techniques for temperature monitoring during laser-induced thermotherapy: an overview. Int J Hyperth 29(7):609–619
15. Bednarkiewicz A, Trejgis K, Drabik J, Kowalczyk A, Marciniak L (2017) Phosphor-assisted temperature sensing and imaging using resonant and nonresonant photoexcitation scheme. ACS Appl Mater Interfaces 9(49):43081–43089. https://doi.org/10.1021/acsami.7b13649
16. Patent RU120008
17. Kholodtsova MN, Grachev PV, Savelieva TA, Kalyagina NA, Blondel W, Loschenov VB (2014) Scattered and fluorescent photon track reconstruction in a biological tissue. Int J Photoenergy. https://doi.org/10.1155/2014/517510
18. Cui W, Kumar C, Chance B (1991) Experimental study of migration depth for the photons measured at sample surface. Proc SPIE 1431:180–191
19. Paterson MS, Chance B, Wilson C (1989) Time resolved reflectance and transmittance for the noninvasive measurement of tissue optical properties. Appl Opt 28:2331
20. Goertzl G, Kalos MH (1958) Monte Carlo in transport problems. In: Hughes DJ, Sanders JE, Horowitz J (eds) Physics and mathematics. Pergamon Press, London
21. Carter LL, Cashwell ED (1977) Particle-transport simulation with Monte carlo method. Nat. Tech. Info. Service TID:26607
22. Krishnaswamy et al. A study on skin optics. Technical Report CS-2004-01.14
23. Bashkatov AN et al (2005) Optical properties of human skin, subcutaneous and mucous tissue in the wavelength range from 400 to 2000nm. J Phys D Appl Phys 38:2543–2555
24. Nielsen KP et al (2008) The optics of human skin: aspects important for human health solar radiation and human. Health 1:35–46
25. Vanetsev A, Kaldvee K, Puust L, Keevend K, Nefedova A, Fedorenko S, Baranchikov A, Sildos I, Rähn M, Sammelselg V, Orlovskii Y (2017) Relation of crystallinity and fluorescent properties of LaF3:Nd3+ nanoparticles synthesized with different water-based techniques. ChemistrySelect 2(17):4874–4881
26. Flock ST, Jacques SL, Wilson BC, Star WM, van Gemert MJC (1992) Optical properties of intralipid: a phantom medium for light propagation studies. Lasers Surg Med 12:510–519
27. van Staveren HG, Moes CJM, van Marle J, Prahl SA, van Gemert MJC (1991) Light scattering in Intralipid-10% in the wavelength range of 400-1100 nanometers. Appl Opt 30:4507–4514
28. Michels R, Foschum F, Kienle A (2008) Optical properties of fat emulsions. Opt Express 16:5907–5925
29. Svelto O (1989) Principles of lasers, 3rd edn. Plenum Publishing Corporation, New York
30. Carnall WT, Goodman GL, Rajnak K, Rana RS (1989) A systematic analysis of the spectra of the lanthanides doped into single crystal LaF3. J Chem Phys 90:3443
31. Carlos LD, Palacio F (2016) Thermometry at the nanoscale: Techniques and Selected Applications The Royal Society of Chemistry, London
32. Sassaroli E, Li KCP, O'Neill BE (2009) Numerical investigation of heating of a gold nanoparticle and the surrounding microenvironment by nanosecond laser pulses for nanomedicine applications. Phys Med Biol 54(18):5541–5560. https://doi.org/10.1088/0031-9155/54/18/013